Angewandte Chemie
Eine Zeitschrift der Gesellschaft Deutscher Chemiker

Supporting Information

PST-24: A Zeolite with Varying Intracrystalline Channel Dimensionality

Donghui Jo[+], Jingjing Zhao[+], Jung Cho[+], Jeong Hwan Lee, Yang Liu, Chang-jun Liu, Xiaodong Zou, and Suk Bong Hong**

anie_202007804_sm_miscellaneous_information.pdf

Experimental Section

Zeolite Synthesis

The reagents, including pentamethylimidazolium hydroxide (PMIOH), were prepared and characterized as previously described.[S1] They are hydrofluoric acid (HF, 48% aqueous solution, J.T. Baker), tetraethylorthosilicate (TEOS, 98%, Aldrich), aluminum hydroxide ($Al(OH)_3 \cdot H_2O$, Aldrich), and deionized water. PMI^+-mediated synthesis of zeolites in fluoride media was carried out using synthesis mixtures with the chemical composition $0.5ROH \cdot xHF \cdot 1.0SiO_2 \cdot yAl_2O_3 \cdot 5.0H_2O$, where R is PMI^+ and x and y are varied between $0.25 \leq x \leq 2.0$ and $0 \leq y \leq 0.1$, respectively. In a typical synthesis, aluminum hydroxide was mixed with a solution of PMIOH and stirred at room temperature for 1 h. To this solution, a given amount of TEOS was added and the mixture was stirred at room temperature for 3 h. The resulting mixture was heated at 80 °C to remove ethanol molecules generated by the hydrolysis of TEOS and some water to obtain the desired composition. Then, an appropriate amount of HF was added while mixing with a spatula. The final synthesis mixture was transferred into a Teflon-lined 23 mL-autoclave and heated under rotation (60 rpm) at 175 °C for 14 days.

The solid products were recovered by filtration or centrifugation, washed repeatedly with water and dried overnight at room temperature. If required, as-made zeolites were converted into their proton form by calcination at 600 °C in air for 8 h. For comparison, the ammonium form of ZSM-5 with Si/Al = 95 were obtained from Tosoh and were converted into their proton form by twice refluxing in 1.0 M NH_4NO_3 solutions for 6 h followed by calcination at 550 °C in air for 2 h.

Characterization

Powder X-ray diffraction (PXRD) patterns were recorded on a PANalytical X´Pert diffractometer (Cu Kα radiation) with an X´Celerator detector. Data were collected with a fixed divergence slit (0.50°) and Soller slits (incident and diffracted = 0.04 rad). Elemental analysis for Si and Al was carried out using a Shimadzu ICPE-9000 inductively coupled plasma spectrometer. The C, H, and N contents of the samples were analyzed by using a Vario EL III elemental organic analyzer. Thermogravimetric analyses (TGA) were performed in air on an SII EXSTAR 6000 thermal analyzer, where the weight losses related to the combustion of OSDAs were further confirmed by differential analyses (DTA) using the same analyzer. Crystal morphology and average size were determined using a JEOL JSM-6510 scanning electron microscopy (SEM). N_2 sorption experiments were carried out on a Mirae SI nanoPorosity-XG analyzer. NH_3 temperature-programmed desorption (TPD) was carried out on a fixed bed, flow-type apparatus linked to a Hewlett-Packard 5890 series II gas chromatograph with a thermal conductivity detector. A sample of ca. 0.1 g was activated in flowing He (50 mL min^{-1}) at 550 °C for 2 h. Then, 10% NH_3 was passed over the sample at 150 °C for 0.5 h. The treated sample was subsequently purged with He at the same temperature for 1 h to remove physisorbed NH_3. Finally, the TPD was performed in flowing He (30 mL min^{-1}) from 150 to 750 °C at a temperature ramp of 10 °C min^{-1}.

^1H and ^{13}C solution nuclear magnetic resonance (NMR) measurements on the iodide form of the PMI^+ cation were performed in 5 mm quartz tubes using a Bruker AVANCE III 300 spectrometer. The ^1H NMR spectra were measured at a ^1H frequency of 300.13 MHz with a π/2 rad pulse length of 11.0 μs and a recycle delay of 2.0 s. The ^{13}C NMR spectra were recorded at a

^{13}C frequency of 75.475 MHz with a $\pi/2$ rad pulse length of 10.2 μs and a recycle delay of 1.5 s. To measure ^{13}C solution NMR spectrum of the organic structure-directing agents (OSDAs) liberated from as-made PST-24, we dissolved the as-made zeolite of 0.5 g in HF (48% aqueous solution, 1.3 mL) and diluted the solution with 2 mL of D_2O.[S2] Solid-state multinuclear NMR measurements were carried out using a Bruker AVANCE III 500 HD spectrometer. The ^{19}F magic-angle-spinning (MAS) NMR spectra were obtained at a spinning rate of 10 kHz, a ^{19}F frequency of 470.54 MHz with a $\pi/2$ rad pulse length of 2.0 μs, a recycle delay of 2.0 s, and an acquisition of 256 pulse transients. The ^{19}F chemical shifts are referenced relative to $CFCl_3$. The ^{1}H-^{13}C cross polarization (CP) MAS NMR spectra were measured at a spinning rate of 20 kHz, a ^{13}C frequency of 125.79 MHz with a $\pi/2$ rad pulse length of 1.8 μs, a contact time of 2.0 ms, a recycle delay of 5.0 s, and an acquisition of ca. 7000 pulse transients. The ^{29}Si MAS NMR spectra were recorded at a spinning rate of 20 kHz, a ^{29}Si frequency of 99.377 MHz with a $\pi/2$ rad pulse length of 4 μs, recycle delay of 150 and 300 s for as-made and calcined PST-24 zeolites, respectively. Approximately 500 pulse transients were accumulated. The ^{13}C and ^{29}Si shifts are referenced relative to TMS.

Structural Analysis

Both as-made and calcined PST-24 samples were investigated by TEM. The samples were crushed in a mortar and dispersed in ethanol. The suspension was then treated by ultrasonication for ca. 30 s. Three droplets from the suspension were applied on a lacey carbon TEM grid (Okenshoji). Continuous rotation electron diffraction (cRED) data were collected on a 200 kV JEOL JEM-2100 LaB_6 TEM at room temperature. The spot size and camera length were 3 and 30 cm, respectively. Video frames of selected area electron diffraction patterns were recorded by a high-speed hybrid camera (Timpix Quad). The rotation speed of the goniometer was 0.23° s^{-1} and the exposure time was 0.5 s, covering 0.46° per frame. cRED data were collected from different crystals, and the total rotation angle of each data sets ranged between 70° and 115°. The cRED data were first processed using the software REDp[S3,S4] for the initial determination of unit cell parameters and space group. Then, the cRED data were processed by the program package XDS[S5], where the instrumental parameters (rotation axis, beam position, and beam orientation), unit cell, orientation matrix, and intensity profiles were refined, and the intensities were integrated. Data sets from different crystals were merged together by XSCALE in XDS. The resulting reflection list $|F(hkl)|^2$ was used by the program SHELX[S6] for structure solution and refinement. The unit cell parameters refined using the PXRD data are more accurate than those from cRED data, and were therefore used in the refinement against cRED data. Based on the reflection conditions, three possible space groups are deduced, *C*2 (No. 5), *Cm* (No. 8), and *C*2/*m* (No. 12). Using space groups *C*2 and *C*2/*m*, it was possible to solve the average structure from the cRED data by direct methods using the program SHELXT.[S6] Further structure refinement against cRED data merged from three crystals shows that *C*2/*m* gave a framework model with the best bond geometry. In order to take into account the disorder of the double 5-ring (*d*5*r*) columns during the refinement, the atoms belonging to the *d*5*r* unit are with an occupancy of 0.5. Soft restraints were applied on the Si-O (1.61 Å) and O…O distances (2.62 Å). Basic experimental parameters for cRED data collection, crystallographic data and detailed refinement results are given in Table S1.

A through-focus[S7] series of 17 HRTEM images were recorded on a Gatan 2k × 2k charge-coupled device camera on a JEOL-2100F TEM at 200 kV. The focus step was -53.3 Å and the exposure time was 5 s per image. The structure projection reconstruction was performed using the

software QFocus[S8]. The starting defocus was determined to be -183 Å and the twofold astigmatism to be 188 Å with azimuth angles of 117°.

Synchrotron PXRD data for PST-24 were collected on the 9B beamline equipped with a ceramic furnace at the Pohang Acceleration Laboratory (PAL; Pohang, Korea) using monochromated X-rays (λ = 1.5175 Å). The detector arm of the vertical scan diffractometer consists of seven sets of Soller slits, flat Ge(111) crystal analyzers, anti-scatter baffles, and scintillation detectors, with each set separated by 20°. Data were obtained on the sample at room temperature in flat plate mode, with a step size of 0.02° and overlaps of 0.5° to the next detector bank. The fractional coordinates of the PST-24 structure obtained from cRED analysis were refined along with the unit cell and instrumental parameters against the synchrotron PXRD data, via the Rietveld method[S9] using the GSAS suite of programs[S10] and EXPGUI graphical interface,[S11] while excluding the region of broad diffraction peaks (2θ < 12°). During the refinements, the framework Si-O and O…O distances were soft-constrained to 1.60 Å (σ = 0.05 Å) and 2.62 Å (σ = 0.05 Å), respectively.[S12] Peak shape was modeled using the pseudo-Voigt profile function.[S13] The isotropic atomic displacement parameters of the framework atoms have been constrained in groups, according to the type of atoms (Si or O) and occupancy (1 or 0.5). The convergence was achieved by refining simultaneously all profile parameters, scale factor, lattice constants, 2θ zero-point, and atomic positions, thermal displacement parameters, and occupancy factors for the framework atoms. The data collection and crystallographic parameters are summarized in Tables S2-S5. The final Rietveld plot, which is displayed in Figure S6, provides a reasonable match between the observed and simulated PXRD patterns. The dimensions of the pore opening are calculated using an oxygen radius of 1.35 Å.

Three different polytypes of PST-24 were built from the refined average structure, and their symmetries were identified by the 'Find Symmetry' tool implemented in the Materials Studio[S14] (Figure S10 and Table S6). Their framework energies relative to α-quartz[S15] were calculated using the Sanders-Leslie-Catlow potential[S16] in the GULP program[S17].

Simulation of ED and PXRD Patterns Using a Supercell

An in-house script was written to generate a supercell model with a random distribution of each disorder type. The script, which is available on github (chojy8300), can read atomic coordinates from a crystallographic information file (cif) and require each unit to be written as a separate file. All *d5r* coordinates were output as cifs that were then distributed throughout the structure with a Monte Carlo algorithm to have a uniform distribution of arrangements S and D. The code can be easily modified to generate a desired supercell dimension. For this work, a $10a \times 1b \times 10c$ supercell (b = 10.1696 Å) of calcined PST-24 was constructed automatically, while utilizing the DLS76 optimized atomic coordinates. The simulated kinematical diffraction intensities of the ED and PXRD patterns were generated using the supercell by CrystDiff[S18] and Materials Studio[S14], respectively (Figures S5e,f and S7).

Molecular Modeling of Intrazeolitic OSDAs

A free PMI^+ ion was optimized using DMol3 with PW91 generalized gradient approximation exchange-correlation function convergent within 10^{-4} Ha, as implemented in Material Studio. Then, the PMI^+ ions were manually introduced in an ordered PST-24 structure (polytype PST-24A) so that themselves alternate with the *d5r* units along the *d5r* columns while accounting for chemical

sensibility. The configuration of the PMI^+ ions was optimized using Dreiding force field[S19] in the GULP program (Figure S9). Only dispersion contributions were assessed.

Catalysis

Catalytic experiments were conducted at atmospheric pressure in a continuous-flow apparatus with a fixed-bed microreactor. The dehydration of 1,3-butanediol was conducted at 300 °C with a weight hourly space velocity of 1.4 h^{-1}. Before the experiments, each catalyst was pretreated under N_2 flow (50 mL min^{-1}) at 500 °C for 2 h and kept at 300 °C to define a standard operating procedure, allowing time for the reactant/carrier gas distribution to stabilize. A reactant stream of 10 wt% aqueous solution of 1,3-butanediol (99%, Alfa) was then fed at a rate of 1.4 mL h^{-1} into the reactor containing 0.1 g of the catalyst. The total gas flow at the reactor inlet was kept constant at 30 mL min^{-1}. The reaction products were analyzed online in an Agilent 7890A gas chromatograph equipped with a HP-5 capillary column (30 m × 0.25 mm) and an FID, with the first analysis carried out after 30 min on stream. The conversion of 1,3-butanediol was defined as the percentage of 1,3-butanediol consumed during the reaction, and the yield of each product was calculated as the percentage of the amount of 1,3-butnaediol converted to reaction products.

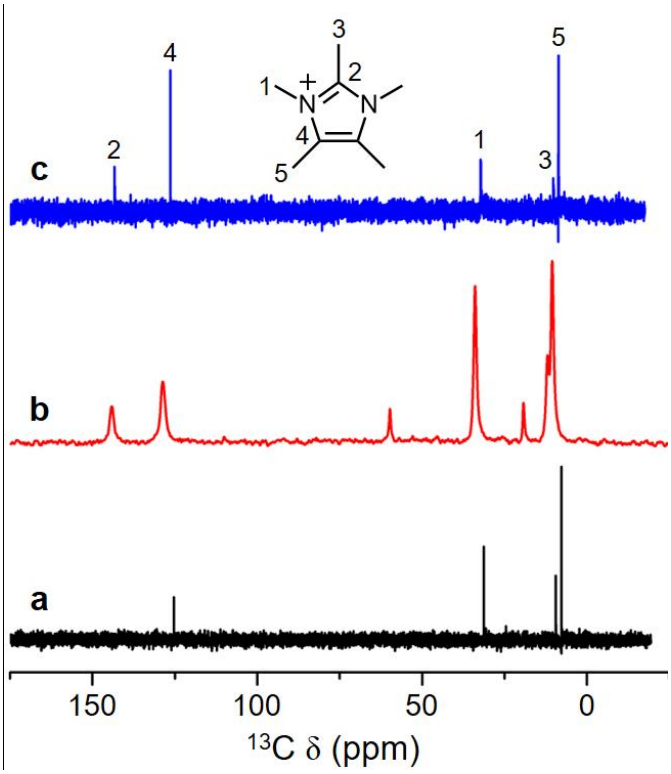

Figure S1. ^{13}C NMR spectra of OSDA, PMI^+: a) ^{13}C NMR of a D_2O solution of the iodide form of PMI^+, b) ^{1}H-^{13}C CP MAS NMR of as-made, pure-silica PST-24 with PMI^+ occluded in the pores, and c) ^{13}C NMR of as-made PST-24 dissolved in HF. These data reveal that the ^{13}C resonances around 19 and 60 ppm (indicated by arrows) in the ^{1}H-^{13}C CP MAS NMR spectrum of as-made PST-24 may also originate from the occluded organic species rather than from the decomposed ones. It should be noted that the resonance due to the imidazolium ring carbon atom at position 2 in PMI^+ is not observed in the solution spectrum a), probably because of the reduced nuclear Overhauser enhancement. The appearance of this resonance in the solution spectrum c) seems to be due to the low pH of the solution of HF-dissolved as-made PST-24.

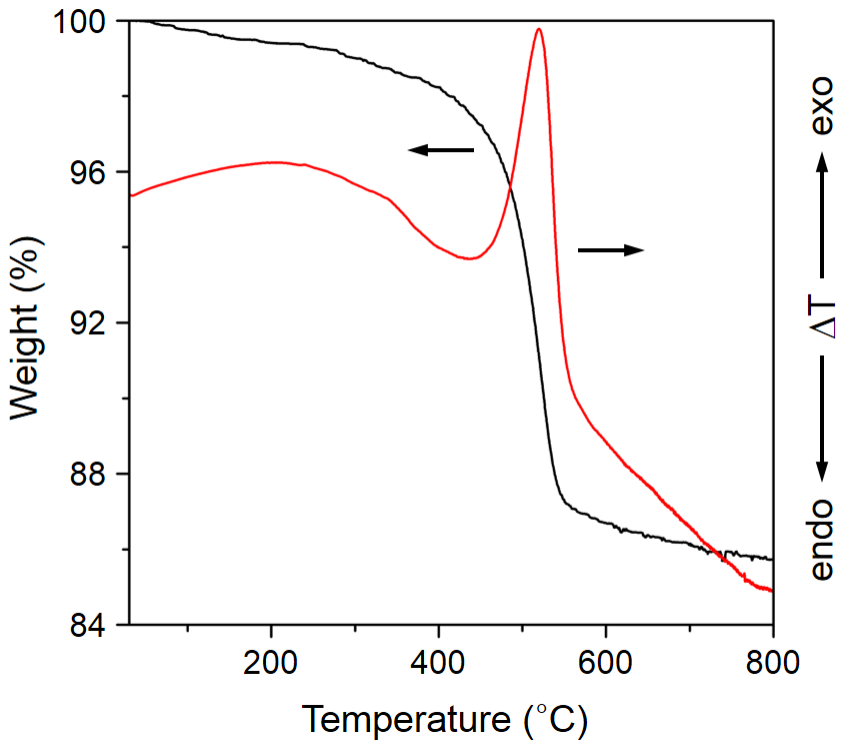

Figure S2. TGA/DTA profiles of as-made, pure-silica PST-24.

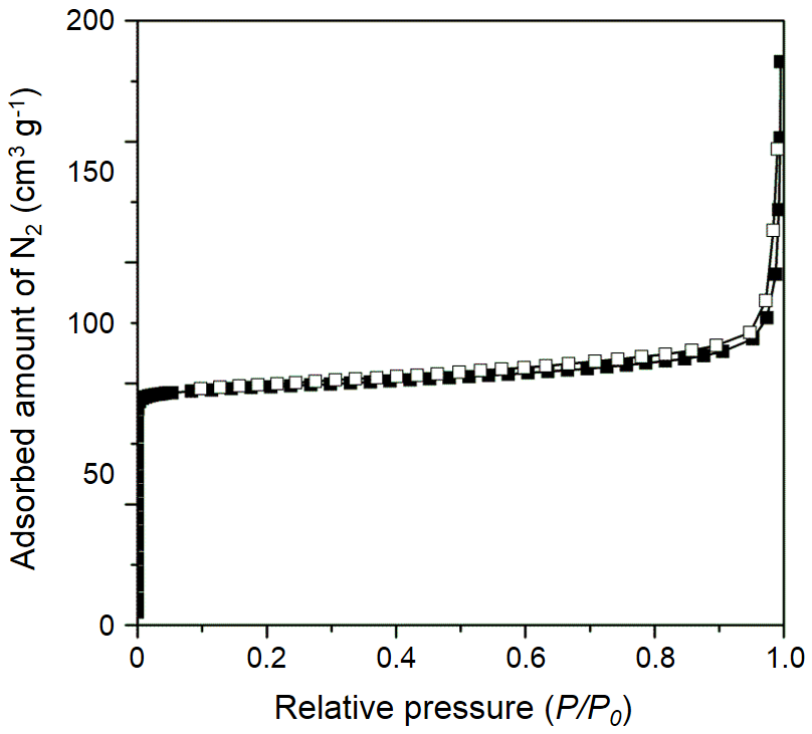

Figure S3. N_2 adsorption (closed) and desorption (open) isotherm of the calcined, pure-silica PST-24. Its BET surface area and micropore volume were calculated to be 390 (microporous, 360; external, 30) $m^2\ g^{-1}$ and 0.14 $cm^3\ g^{-1}$, respectively.

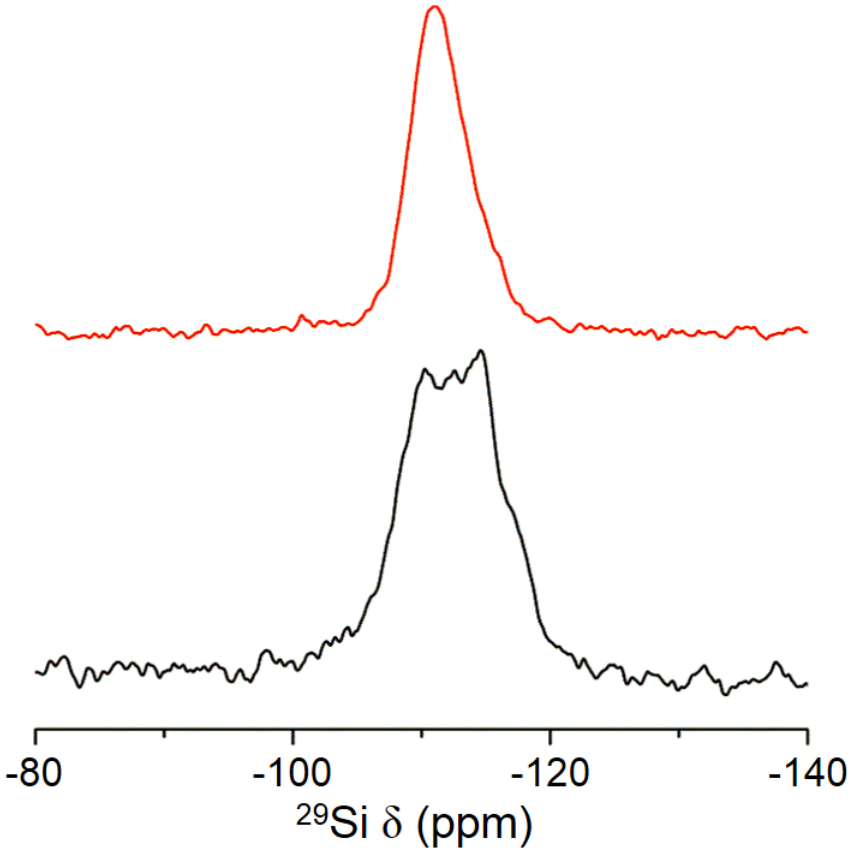

Figure S4. ^{29}Si MAS NMR spectra of the as-made (black) and calcined (red) forms of pure-silica PST-24.

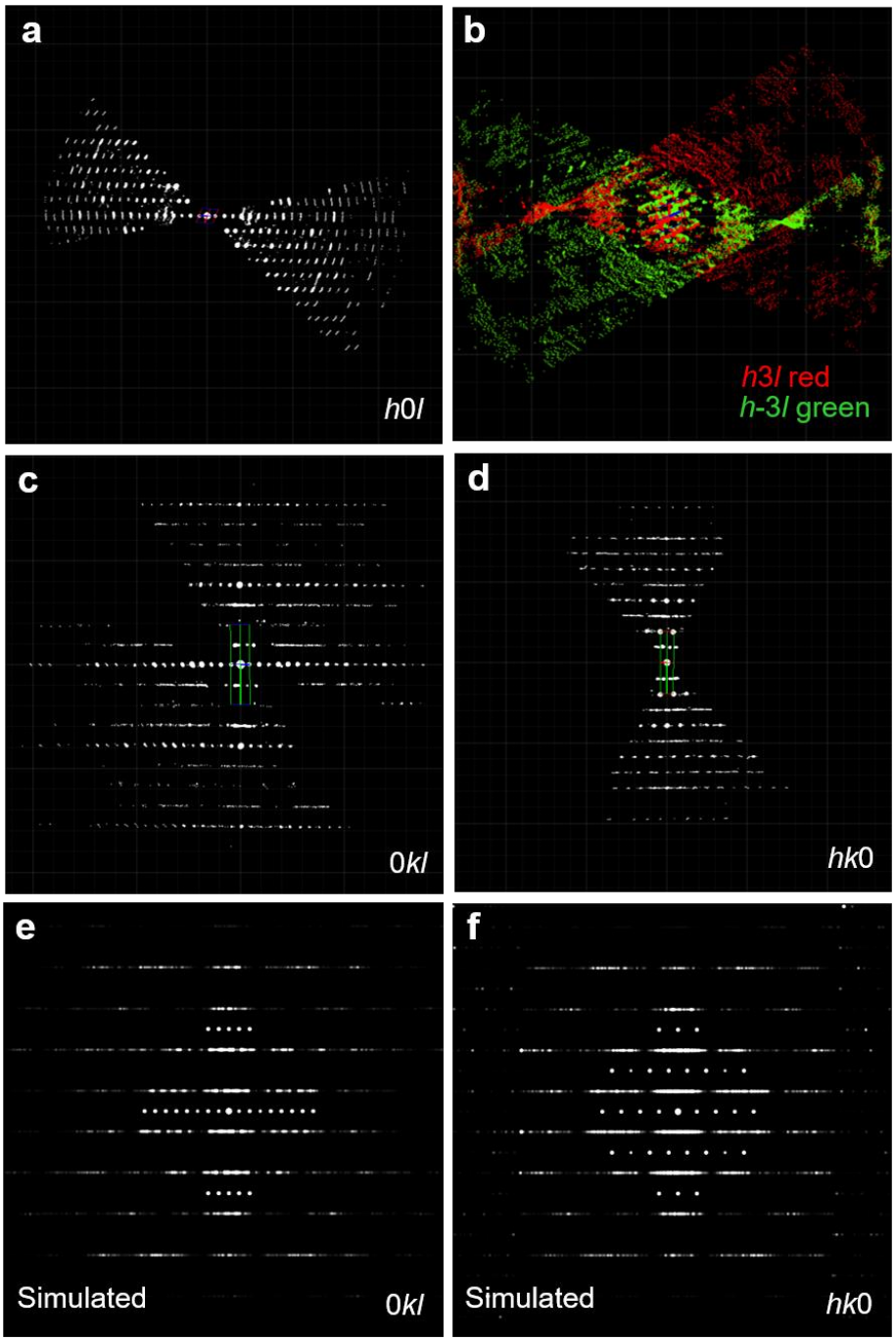

Figure S5. a)-d) 2D slices of *h*0*l*, *h*±3*l*, 0*kl*, and *hk*0 reciprocal lattice planes reconstructed from the cRED data of calcined, pure-silica PST-24. The *h*3*l* and *h*-3*l* planes show that the diffuse scattering is quite random without any specific rules. e), f) Simulated 0*kl* and *hk*0 diffraction patterns by CrystDiff from a 10*a* × 1*b* × 10*c* supercell containing a random distribution of arrangements S and D. The supercell was generated by a Monte Carlo algorithm. The experimental and simulated diffraction patterns show a good agreement with each other, despite the limited size of the supercell used for this simulation.

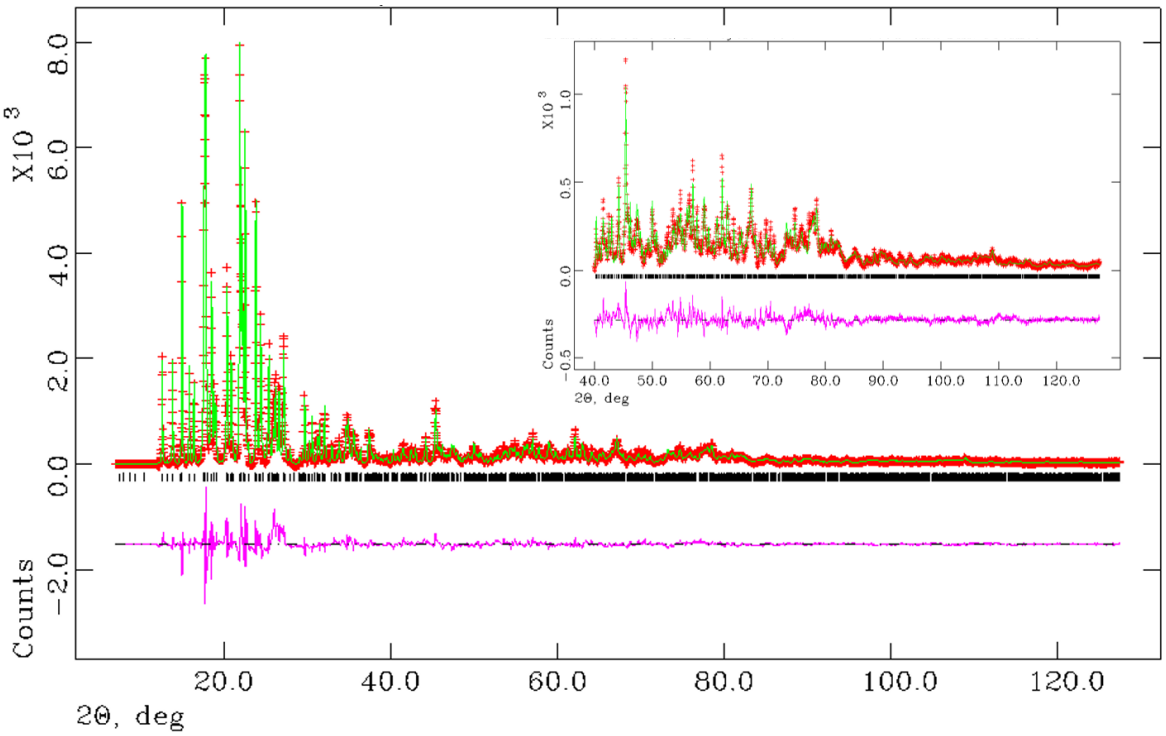

Figure S6. Rietveld plot of calcined, pure-silica PST-24 ($\lambda = 1.5175$ Å; $2\theta \geq 12°$): observed data (+), calculated fit (solid line), and difference plot (lower trace). The tick marks represent the positions of allowed reflections.

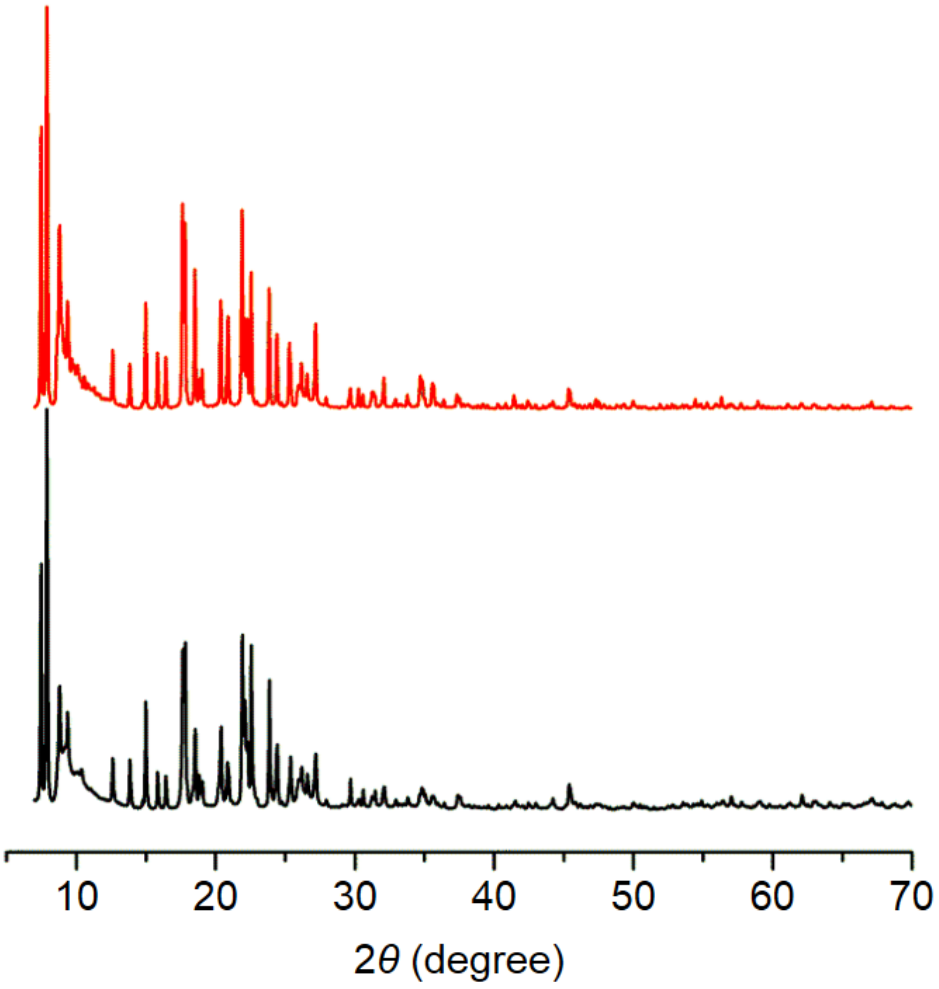

Figure S7. The experimental (black) and simulated (red) PXRD patterns of calcined, pure-silica PST-24 (λ = 1.5175 Å). The simulation was carried out by Materials Studio from a 10*a* × 1*b* × 10*c* supercell.

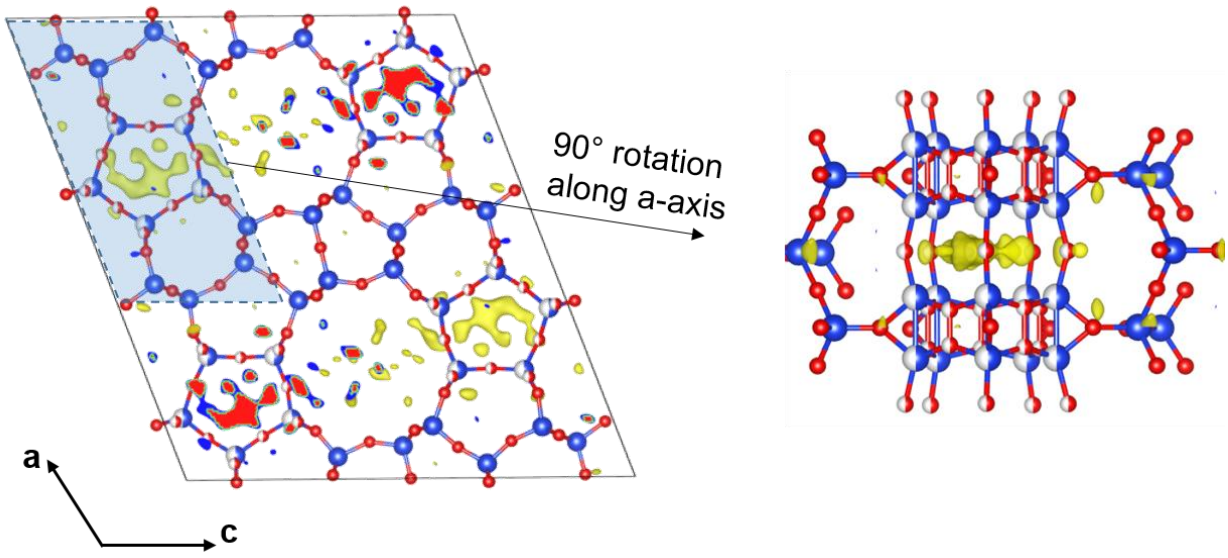

Figure S8. Difference Fourier map (F_o - F_c) of average structure of as-made, pure-silica PST-24 refined against the cRED data. The positive map (yellow) was countered at the isosurface level of 0.45.

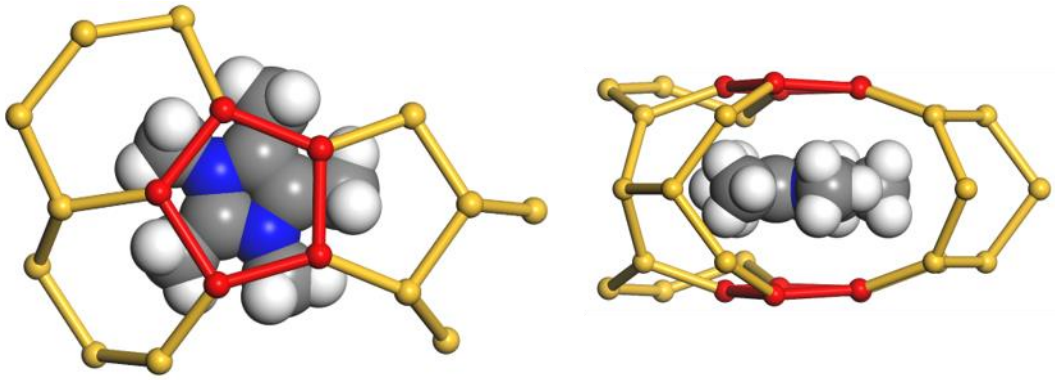

Figure S9. Energy-minimized configuration of the PMI^+ ion within the sinusoidal 8-ring channel along the *c*-axis of PST-24A. The 5-rings belonging to *d5r* units are marked in red.

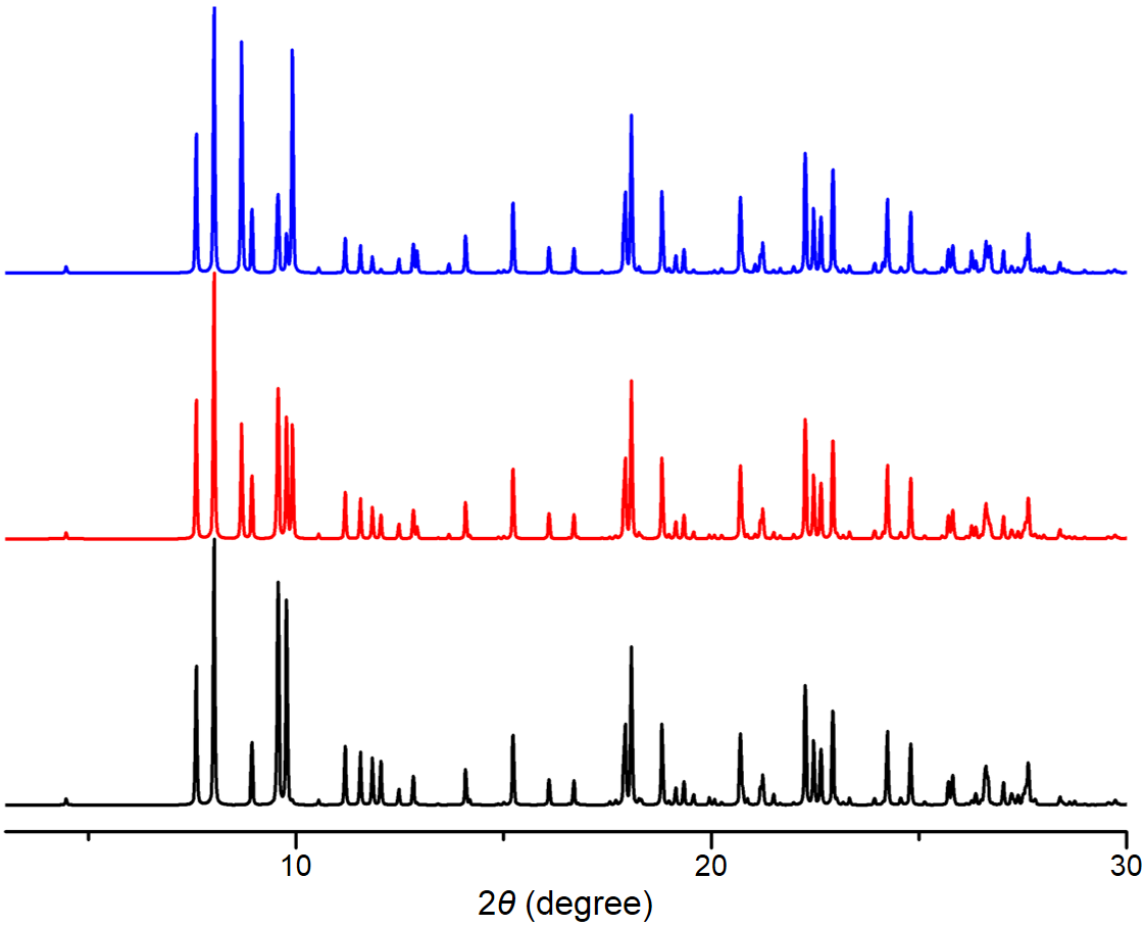

Figure S10. Simulated PXRD patterns of three PST-24 polytypes: (from bottom to top) PST-24A, PST-24B, and PST-24C (λ = 1.54056 Å).

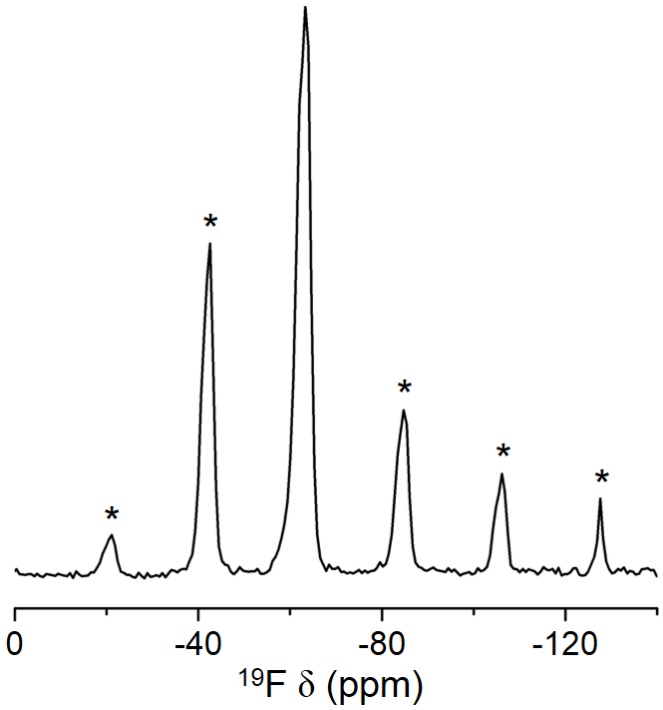

Figure S11. ^{19}F MAS NMR spectrum of as-made, pure-silica PST-24. Spinning side bands are marked by asterisks.

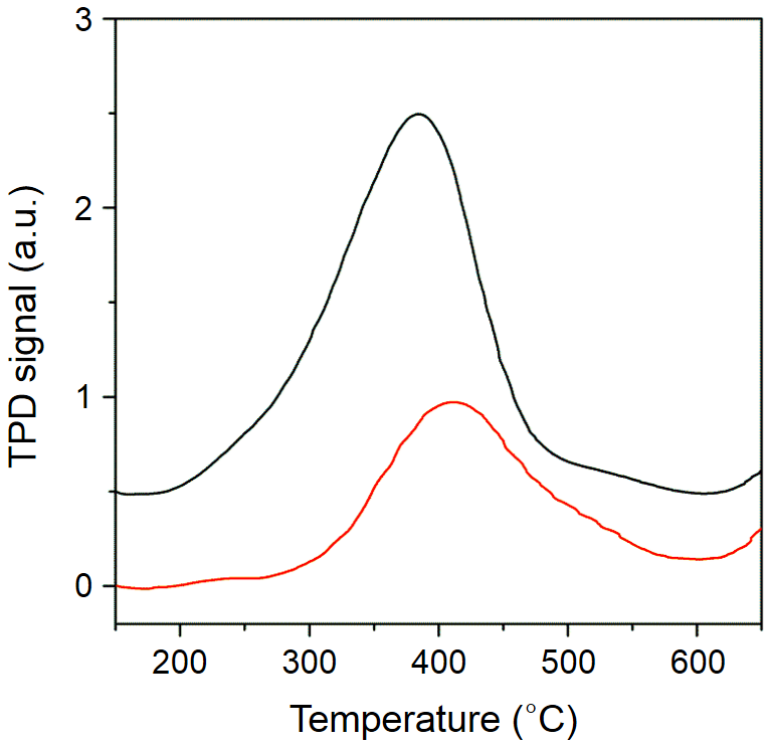

Figure S12. NH_3 TPD profiles for H-ZSM-5 (black) and H-Al-PST-24 (red). The bulk Si/Al ratio of each zeolite is 95 and 200, respectively.

Table S1. Experimental parameters for cRED data collection and crystallographic information for the averaged structures of the as-made and calcined forms of pure-silica PST-24.[a]

Sample	As-made PST-24	Calcined PST-24
Wavelength (Å)	0.0251	0.0251
Rotation range (°)	70-115	70-110
Rotation speed (°/s)	0.23	0.23
Exposure time/frame (s)	0.5	0.5
No. of data sets	7	3
Crystal width (nm)	100-200	100-200
Resolution (Å)	0.90	0.90
Crystal system	Monoclinic	Monoclinic
Space group	*C*2/*m* (No. 12)	*C*2/*m* (No. 12)
Unit cell parameters (cRED)		
a (Å)	24.313(44)	24.140(44)
b (Å)	5.384(2)	5.211(18)
c (Å)	22.016(39)	21.761(30)
β (°)	111.422(190)	111.389(180)
Completeness	0.846	0.918
Total reflections	12752	7374
R_{int}	0.2583	0.1797
No. unique reflections I > 2σ (I)/all	1391/1642	1469/1788
No. of parameters	113	111
No. of restrains	57	87
R_1(F > 4σ(F))/R_1(all)	0.2148/0.2387	0.3387/0.3684
GOF	2.102	3.072

[a] The unit cell parameters, obtained by the Pawley and Rietveld (see Table S2) fits of the as-made (lab) and calcined (synchrotron) PXRD patterns, respectively, were used for the structure refinement. The unit cell parameters from the cRED data are slightly larger than those from the PXRD data, presumably due to lens distortions and the sample height changing during the data collection.

Table S2. Crystallographic and experimental parameters for the Rietveld refinement of calcined, pure-silica PST-24.

Unit cell composition	$\|(H_2O)_{1.6}\|[Si_{44}O_{88}]$
Refined structure	$[Si_{44}O_{88}]$
Crystal system	Monoclinic
Space group	*C*2/*m* (No. 12)
a (Å)	23.7125(6)
b (Å)	5.0848(2)
c (Å)	21.3024(6)
β (°)	111.838(2)
Unit cell volume (Å^3)	2384.2(1)
X-ray source	9B beamline, PAL
Wavelength (Å)	1.5175
Step size (°)	0.02
2*θ* scan range (°)	7-127.5
No. of contributing reflections	2298
No. of restraints	118
No. of parameters	117
R_{wp} (%)	9.17
R_F^2 (%)	11.1
χ^2	6.59

Table S3. Atomic coordinates and thermal parameters for calcined, pure-silica PST-24 refined by the Rietveld method.

Atom	*x*	*y*	*z*	Occupancy	U_{iso} (× 100 Å^2)	Multiplicity
Si1	0.42429(32)	0	0.0972(4)	1	1.66(5)	4
Si2	0.38123(32)	0.5	0.3996(4)	1	1.66(5)	4
Si3	0.46729(31)	0.5	0.3188(4)	1	1.66(5)	4
Si4	0.38746(32)	0.5	0.16045(35)	1	1.66(5)	4
Si5	0.56741(32)	1	0.5073(4)	1	1.66(5)	4
Si6	0.55024(32)	1	0.3568(4)	1	1.66(5)	4
Si7	0.55013(33)	0.1962(15)	0.1286(4)	0.5	1.56(10)	8
Si8	0.6346(4)	0.1877(15)	0.0476(4)	0.5	1.56(10)	8
Si9	0.76506(31)	0.1945(14)	0.1595(4)	0.5	1.56(10)	8
Si10	0.26382(35)	0.3024(15)	0.3031(4)	0.5	1.56(10)	8
Si11	0.12859(34)	0.3023(15)	0.2859(4)	0.5	1.56(10)	8
O1	0.3995(4)	0.7428(9)	0.45164(31)	1	3.51(13)	8
O2	0.40668(31)	0.2433(9)	0.13216(30)	1	3.51(13)	8
O3	0.50489(28)	0.7596(9)	0.3301(4)	1	3.51(13)	8
O4	0.3811(4)	0	0.01741(25)	1	3.51(13)	4
O5	0.81598(21)	0	0.1490(4)	1	3.51(13)	4
O6	0.49336(21)	0	0.1085(5)	1	3.51(13)	4
O7	0.4239(5)	0.5	0.2407(4)	1	3.51(13)	4
O8	0.31137(26)	0.5	0.3556(4)	1	3.51(13)	4
O9	0.42134(28)	0.5	0.3552(4)	1	3.51(13)	4
O10	0.60101(24)	1	0.32584(26)	1	3.51(13)	4
O11	0.5790(4)	1	0.43870(27)	1	3.51(13)	4
O12	0.5	1	0.5	1	3.51(13)	2
O13	0.70090(23)	0.1182(18)	0.10094(33)	0.5	2.54(31)	8
O14	0.75636(30)	0.0994(21)	0.22656(21)	0.5	2.54(31)	8
O15	0.19694(19)	0.3830(18)	0.3019(4)	0.5	2.54(31)	8
O16	0.59584(35)	0.1243(18)	0.20537(23)	0.5	2.54(31)	8
O17	0.59124(21)	0.1085(18)	0.08667(24)	0.5	2.54(31)	8
O18	0.2774(7)	0	0.3260(13)	0.5	2.54(31)	4
O19	0.1217(6)	0	0.2976(7)	0.5	2.54(31)	4
O20	0.7799(6)	0.5	0.1577(8)	0.5	2.54(31)	4
O21	0.6310(7)	0.5	0.0302(7)	0.5	2.54(31)	4
O22	0.5335(6)	0.5	0.1199(8)	0.5	2.54(31)	4

Table S4. Bond lengths for calcined, pure-silica PST-24 refined by the Rietveld method.

Bond length (Å)	
Si1-O2 (×2)	1.577(8)
Si1-O4	1.627(8)
Si1-O6	1.565(9)
Si2-O1 (×2)	1.607(7)
Si2-O8	1.571(8)
Si2-O9	1.571(12)
Si3-O3 (×2)	1.561(6)
Si3-O7	1.598(9)
Si3-O9	1.555(12)
Si4-O2 (×2)	1.575(8)
Si4-O5	1.620(9)
Si4-O7	1.604(9)
Si5-O1 (×2)	1.606(6)
Si5-O11	1.585(11)
Si5-O12	1.547(8)
Si6-O3 (×2)	1.587(7)
Si6-O10	1.573(11)
Si6-O11	1.621(9)
Si7-O6	1.600(8)
Si7-O16	1.632(9)
Si7-O17	1.611(11)
Si7-O22	1.588(8)
Si8-O4	1.608(9)
Si8-O13	1.599(9)
Si8-O17	1.597(11)
Si8-O21	1.625(8)
Si9-O5	1.639(10)
Si9-O13	1.616(8)
Si9-O14	1.592(11)
Si9-O20	1.596(8)
Si10-O8	1.610(8)
Si10-O14	1.651(10)
Si10-O15	1.629(10)
Si10-O18	1.609(10)
Si11-O10	1.605(10)
Si11-O15	1.581(9)
Si11-O16	1.642(9)
Si11-O19	1.576(8)
Si-O (Avg.)	1.597

Table S5. Bond angles for calcined, pure-silica PST-24 refined by the Rietveld method.

Bond angle (°)			
O2-Si1-O2	103.3(7)	Si1-O2-Si4 (×2)	174.6(5)
O2-Si1-O4 (×2)	108.6(4)	Si1-O4-Si8	139.0(4)
O2-Si1-O6 (×2)	111.9(4)	Si1-O6-Si7	140.3(4)
O4-Si1-O6	112.1(7)	Si2-O9-Si3	173.6(5)
O1-Si2-O1	100.4(6)	Si2-O1-Si5 (×2)	162.4(8)
O1-Si2-O8 (×2)	111.5(5)	Si2-O8-Si10	136.5(4)
O1-Si2-O9 (×2)	110.3(5)	Si3-O9-Si2	173.6(5)
O8-Si2-O9	112.3(6)	Si3-O7-Si4	173.2(9)
O3-Si3-O3	115.5(6)	Si3-O3-Si6 (×2)	168.2(6)
O3-Si3-O7 (×2)	105.7(5)	Si4-O2-Si1 (×2)	174.6(5)
O3-Si3-O9 (×2)	112.9(5)	Si4-O7-Si3	173.2(9)
O7-Si3-O9	102.7(6)	Si4-O5-Si9	139.6(3)
O2-Si4-O2	112.0(7)	Si5-O1-Si2 (×2)	162.4(8)
O2-Si4-O5 (×2)	112.2(4)	Si5-O12-Si5	180
O2-Si4-O7 (×2)	106.9(4)	Si5-O11-Si6	147.7(7)
O5-Si4-O7	106.1(7)	Si6-O3-Si3 (×2)	168.2(6)
O1-Si5-O1	109.0(5)	Si6-O11-Si11	147.7(7)
O1-Si5-O11 (×2)	106.6(5)	Si6-O10-Si11	138.4(3)
O1-Si5-O12 (×2)	109.4(5)	Si7-O6-Si1	140.3(4)
O11-Si5-O12	115.8(5)	Si7-O22-Si7	153.2(10)
O3-Si6-O3	100.7(5)	Si7-O17-Si8	149.2(7)
O3-Si6-O10 (×2)	111.9(5)	Si7-O16-Si11	151.1(7)
O3-Si6-O11 (×2)	110.0(5)	Si8-O4-Si1	139.0(4)
O10-Si6-O11	111.7(5)	Si8-O17-Si7	149.2(7)
O6-Si7-O16	107.9(7)	Si8-O21-Si8	155.3(11)
O6-Si7-O17	107.5(6)	Si8-O13-Si9	152.8(7)
O6-Si7-O22	115.3(7)	Si9-O5-Si4	139.6(3)
O16-Si7-O17	100.4(5)	Si9-O13-Si8	152.8(7)
O16-Si7-O22	112.2(8)	Si9-O20-Si9	153.4(13)
O17-Si7-O22	112.3(9)	Si9-O14-Si10	142.4(8)
O4-Si8-O13	109.4(7)	Si10-O8-Si2	136.5(4)
O4-Si8-O17	108.1(6)	Si10-O14-Si9	142.4(8)
O4-Si8-O21	114.1(7)	Si10-O18-Si10	145.7(16)
O13-Si8-O17	103.2(5)	Si10-O15-Si11	148.4(7)
O13-Si8-O21	109.5(7)	Si11-O10-Si6	138.4(3)
O17-Si8-O21	112.0(9)	Si11-O16-Si7	151.1(7)
O5-Si9-O13	106.2(6)	Si11-O15-Si10	148.4(7)
O5-Si9-O14	106.7(6)	Si11-O19-Si11	154.6(14)
O5-Si9-O20	113.8(8)	Si-O-Si (Avg.)	153.1
O13-Si9-O14	102.8(6)		
O13-Si9-O20	111.5(7)		
O14-Si9-O20	114.9(9)		
O8-Si10-O14	106.7(6)		
O8-Si10-O15	106.3(6)		

O8-Si10-O18	112.1(8)
O14-Si10-O15	99.3(5)
O14-Si10-O18	121.6(12)
O15-Si10-O18	109.2(9)
O10-Si11-O15	108.1(5)
O10-Si11-O16	106.5(5)
O10-Si11-O19	116.1(8)
O15-Si11-O16	102.4(6)
O15-Si11-O19	112.2(8)
O16-Si11-O19	110.5(7)
O-Si-O (Avg.)	109.3

Table S6. Fractional coordinates for polytypes PST-24A, PST-24B, and PST-24C.

PST-24A ($P2_1/c$, a = 25.3037 Å, b = 10.1696 Å, c = 23.7125 Å, β = 128.6057°)

Atom	*x*	*y*	*z*	Atom	*x*	*y*	*z*
Si1	-0.3031	0.0262	0.2107	O12	-0.7734	-0.0755	-0.2798
Si2	-0.2859	0.0262	0.0927	O13	-0.7946	-0.0629	-0.1404
Si3	-0.8714	-0.0269	-0.1715	O14	-0.9133	-0.0708	-0.2545
Si4	-0.9524	-0.0312	-0.337	O15	-0.5484	-0.0036	-0.1979
Si5	-0.8405	-0.0278	-0.3556	O16	-0.8678	0.2467	-0.5245
Si6	-0.8714	0.2231	0.3285	O17	-0.6699	0.0048	0.5752
Si7	-0.9524	0.2189	0.163	O18	-0.8991	0.1841	0.15
Si8	-0.8405	0.2223	0.1444	O19	-0.7734	0.1745	0.2202
Si9	-0.6969	0.2762	-0.2107	O20	-0.6981	0.3165	-0.145
Si10	-0.7141	0.2762	-0.0927	O21	-0.7946	0.1872	0.3596
Si11	-0.0972	-0.125	0.5771	O22	-0.9133	0.1793	0.2455
Si12	-0.0972	0.125	1.0771	O23	-0.0174	-0.125	0.6137
Si13	-0.3996	0.125	0.2316	O24	-0.149	-0.125	0.917
Si14	-0.3188	0.125	0.3985	O25	-0.1085	-0.125	0.6349
Si15	-0.1604	0.125	0.4771	O26	-0.326	-0.125	0.2014
Si16	-0.3996	-0.125	0.7316	O27	-0.2976	-0.125	0.0741
Si17	-0.3188	-0.125	0.8985	O28	-0.0174	0.125	1.1137
Si18	-0.1604	-0.125	0.9771	O29	-0.149	0.125	0.417
Si19	-0.5073	-0.125	0.3101	O30	-0.1085	0.125	1.1349
Si20	-0.3568	-0.125	0.4434	O31	-0.2407	0.125	0.4332
Si21	-0.5073	0.125	-0.1899	O32	-0.3556	0.125	0.2058
Si22	-0.3568	0.125	-0.0566	O33	-0.3552	0.125	0.3161
O1	-0.4516	0.2464	0.1979	O34	-0.2407	-0.125	0.9332
O2	-0.1322	-0.0034	0.5245	O35	-0.3556	-0.125	0.7058
O3	-0.3301	0.2548	0.4248	O36	-0.3552	-0.125	0.8161
O4	-0.3019	0.0665	0.145	O37	-0.1577	-0.125	0.3722
O5	-0.4516	-0.0036	0.6979	O38	-0.0302	-0.125	0.3508
O6	-0.1322	0.2467	1.0245	O39	-0.1199	-0.125	0.1636
O7	-0.3301	0.0048	-0.0752	O40	-0.3258	-0.125	0.5252
O8	-0.5484	0.2464	0.3021	O41	-0.4387	-0.125	0.3903
O9	-0.8678	-0.0034	-0.0245	O42	-0.3258	0.125	0.0252
O10	-0.6699	0.2548	0.0752	O43	-0.4387	0.125	-0.1097
O11	-0.8991	-0.0659	-0.35	O44	-0.5	-0.125	0.25

PST-24B (*P*-1, *a* = 23.7125 Å, *b* = 10.1696 Å, *c* = 21.3024 Å, *β* = 111.8378°)							
Atom	*x*	*y*	*z*	Atom	*x*	*y*	*z*
Si1	0.5501	0.0981	0.1286	O24	0.0933	0.1284	0.8678
Si2	0.6346	0.0939	0.0476	O25	0.9951	0.3702	0.6699
Si3	0.7651	0.0973	0.1595	O26	0.7991	0.1909	0.8991
Si4	0.2638	0.1512	0.3031	O27	0.7436	0.2005	0.7734
Si5	0.1286	0.1512	0.2859	O28	0.9042	0.1879	0.7946
Si6	0.7638	0.4012	0.3031	O29	0.9088	0.1958	0.9133
Si7	0.6286	0.4012	0.2859	O30	0.3995	0.1286	0.4516
Si8	0.7362	0.1512	0.6969	O31	0.4067	0.3784	0.1322
Si9	0.8714	0.1512	0.7141	O32	0.5049	0.1202	0.3301
Si10	0.9499	0.1519	0.8714	O33	0.7009	0.4409	0.1009
Si11	0.8654	0.1562	0.9524	O34	0.7564	0.4505	0.2266
Si12	0.7349	0.1528	0.8405	O35	0.5958	0.4379	0.2054
Si13	0.5501	0.4019	0.1286	O36	0.5912	0.4458	0.0867
Si14	0.6346	0.4062	0.0476	O37	0.8995	0.3786	0.4516
Si15	0.7651	0.4028	0.1595	O38	0.9067	0.1284	0.1322
Si16	0.0501	0.1519	0.1286	O39	0.0049	0.3702	0.3301
Si17	0.1346	0.1562	0.0476	O40	0.2009	0.1909	0.1009
Si18	0.2651	0.1528	0.1595	O41	0.2564	0.2005	0.2266
Si19	0.7638	0.0988	0.3031	O42	0.6969	0.0585	0.3019
Si20	0.6286	0.0989	0.2859	O43	0.0958	0.1879	0.2054
Si21	0.4243	0	0.0972	O44	0.0912	0.1958	0.0867
Si22	0.9243	0.25	0.0972	O45	0.3811	0	0.0174
Si23	0.0757	0.25	0.9028	O46	0.816	0	0.149
Si24	0.3812	0.25	0.3996	O47	0.4934	0	0.1085
Si25	0.4673	0.25	0.3188	O48	0.2774	0	0.326
Si26	0.3875	0.25	0.1604	O49	0.1217	0	0.2976
Si27	0.8812	0	0.3996	O50	0.8811	0.25	0.0174
Si28	0.9673	0	0.3188	O51	0.316	0.25	0.149
Si29	0.8875	0	0.1604	O52	0.9934	0.25	0.1085
Si30	0.6188	0.25	0.6004	O53	0.7774	0.25	0.326
Si31	0.5327	0.25	0.6812	O54	0.6217	0.25	0.2976
Si32	0.6125	0.25	0.8396	O55	0.1189	0.25	0.9826
Si33	0.5674	0	0.5073	O56	0.684	0.25	0.851
Si34	0.5502	0	0.3568	O57	0.0066	0.25	0.8915
Si35	0.0674	0.25	0.5073	O58	0.4239	0.25	0.2407
Si36	0.0502	0.25	0.3568	O59	0.3114	0.25	0.3556
Si37	0.9326	0.25	0.4927	O60	0.4213	0.25	0.3552
Si38	0.9498	0.25	0.6432	O61	0.7799	0.25	0.1577
Si39	0.4243	0.5	0.0972	O62	0.631	0.25	0.0302
Si40	0.8812	0.5	0.3996	O63	0.5335	0.25	0.1199
Si41	0.9673	0.5	0.3188	O64	0.9239	0	0.2407
Si42	0.8875	0.5	0.1604	O65	0.8114	0	0.3556
Si43	0.5674	0.5	0.5073	O66	0.9213	0	0.3552
Si44	0.5502	0.5	0.3568	O67	0.2799	0	0.1577
O1	0.3995	0.3714	0.4516	O68	0.131	0	0.0302
O2	0.4067	0.1217	0.1322	O69	0.0335	0	0.1199
O3	0.5049	0.3798	0.3301	O70	0.5761	0.25	0.7593
O4	0.7009	0.0591	0.1009	O71	0.6886	0.25	0.6444
O5	0.7564	0.0495	0.2266	O72	0.5787	0.25	0.6448
O6	0.1969	0.1915	0.3019	O73	0.601	0	0.3258
O7	0.5958	0.0622	0.2054	O74	0.579	0	0.4387
O8	0.5912	0.0543	0.0867	O75	0.101	0.25	0.3258
O9	0.8995	0.1214	0.4516	O76	0.079	0.25	0.4387

O10	0.9067	0.3717	0.1322	O77	0.899	0.25	0.6742
O11	0.0049	0.1298	0.3301	O78	0.921	0.25	0.5613
O12	0.6969	0.4415	0.3019	O79	0	0.25	0.5
O13	0.6005	0.3714	0.5484	O80	0.3811	0.5	0.0174
O14	0.5933	0.1217	0.8678	O81	0.816	0.5	0.149
O15	0.4951	0.3798	0.6699	O82	0.4934	0.5	0.1085
O16	0.8031	0.1915	0.6981	O83	0.9239	0.5	0.2407
O17	0.1005	0.1214	0.5484	O84	0.8114	0.5	0.3556
O18	0.0933	0.3717	0.8678	O85	0.9213	0.5	0.3552
O19	0.9951	0.1298	0.6699	O86	0.601	0.5	0.3258
O20	0.6005	0.1286	0.5484	O87	0.579	0.5	0.4387
O21	0.5933	0.3784	0.8678	O88	0.5	0	0.5
O22	0.4951	0.1202	0.6699	O89	0.5	0.5	0.5
O23	0.1005	0.3786	0.5484				

PST-24C (*P*2/*c*, *a* = 25.3037 Å, *b* = 10.1696 Å, *c* = 23.7125 Å, *β* = 128.6057°)							
Atom	*x*	*y*	*z*	Atom	*x*	*y*	*z*
Si1	-0.1286	0.2231	0.1715	O13	-0.5484	0.2536	-0.1979
Si2	-0.0476	0.2189	0.337	O14	-0.6699	0.2452	0.5752
Si3	-0.1595	0.2223	0.3556	O15	-0.0174	-0.125	0.6137
Si4	-0.6969	0.2238	0.2893	O16	-0.149	-0.125	0.917
Si5	-0.7141	0.2239	0.4073	O17	-0.1085	-0.125	0.6349
Si6	-0.0972	-0.125	0.5771	O18	-0.2407	0.125	0.4332
Si7	-0.3996	0.125	0.2316	O19	-0.3556	0.125	0.2058
Si8	-0.3188	0.125	0.3985	O20	-0.3552	0.125	0.3161
Si9	-0.1604	0.125	0.4771	O21	-0.3258	-0.125	0.5252
Si10	-0.5073	-0.125	0.3101	O22	-0.4387	-0.125	0.3903
Si11	-0.3568	-0.125	0.4434	O23	-0.1322	0.4967	0.5245
Si12	-0.1286	0.4731	0.6715	O24	-0.1009	0.4341	0.85
Si13	-0.0476	0.4689	0.837	O25	-0.2266	0.4245	0.7798
Si14	-0.1595	0.4723	0.8556	O26	-0.3019	0.5665	0.145
Si15	-0.3031	0.5262	0.2107	O27	-0.2054	0.4372	0.6404
Si16	-0.2859	0.5262	0.0927	O28	-0.0867	0.4293	0.7545
Si17	-0.0972	0.375	0.5771	O29	-0.4516	0.4964	0.6979
Si18	-0.3996	0.625	0.2316	O30	-0.3301	0.5048	-0.0752
Si19	-0.3188	0.625	0.3985	O31	-0.0174	0.375	0.6137
Si20	-0.1604	0.625	0.4771	O32	-0.149	0.375	0.917
Si21	-0.5073	0.375	0.3101	O33	-0.1085	0.375	0.6349
Si22	-0.3568	0.375	0.4434	O34	-0.326	0.375	0.2014
O1	-0.4516	0.2464	0.1979	O35	-0.2976	0.375	0.0741
O2	-0.1322	-0.0034	0.5245	O36	-0.2407	0.625	0.4332
O3	-0.3301	0.2548	0.4248	O37	-0.3556	0.625	0.2058
O4	-0.4516	-0.0036	0.6979	O38	-0.3552	0.625	0.3161
O5	-0.1322	0.2467	1.0245	O39	-0.1577	0.625	0.8722
O6	-0.3301	0.0048	-0.0752	O40	-0.0302	0.625	0.8508
O7	-0.1009	0.1841	0.35	O41	-0.1199	0.625	0.6636
O8	-0.2266	0.1745	0.2798	O42	-0.3258	0.375	0.5252
O9	-0.2054	0.1872	0.1404	O43	-0.4387	0.375	0.3903
O10	-0.0867	0.1793	0.2545	O44	-0.5	-0.125	0.25
O11	-0.8678	0.2534	-0.0245	O45	-0.5	0.375	0.25
O12	-0.6981	0.1835	0.355				

References

[S1] J. E. Schmidt, M. A. Deimund, D. Xie, M. E. Davis, *Chem. Mater.* **2015**, *27*, 3756-3762.

[S2] A. Rojas, O. Arteaga, B. Kahr, M. A. Camblor, *J. Am. Chem. Soc.* **2013**, *135*, 11975-11984.

[S3] W. Wan, J. Sun, J. Su, S. Hovmöller, X. Zou, *J. Appl. Cryst.* **2013**, *46*, 1863-1873.

[S4] D. Zhang; P. Oleynikov, S. Hovmöller; X. Zou. *Z. Kristallogr.* **2010**, *225*, 94-102.

[S5] W, Kabsch, *Acta Cryst.* **2010**, *D66*, 125-132.

[S6] G. M. Sheldrick, *Acta Cryst.* **2015**, *A71*, 3-8.

[S7] E. J. Kirkland, B. M. Siegel, *Ultramicroscopy* **1980**, *5*, 479-503.

[S8] W. Wan, S. Hovmöller, X. Zou, *Ultramicroscopy* **2012**, *115*, 50-60.

[S9] H. M. Rietveld, *J. Appl. Crystallogr.* **1969**, *2*, 65-71.

[S10] A. C. Larson, R. B. Von Dreele, *General Structure Analysis System (GSAS), Los Alamos National Laboratory Report LAUR 86-748*, Los Alamos National Laboratory: Los Alamos, NM, 2004.

[S11] B. H. Toby, *J. Appl. Crystallogr.* **2001**, *34*, 210-213.

[S12] W. H. Baur, R. X. Fischer, *Chem. Mater.* **2019**, *31*, 2401-2420.

[S13] J. B. Hastings, W. Thomlinson, D. E. Cox, *J. Appl. Crystallogr.* **1984**, *17*, 85-95.

[S14] Dassault Systémes BIOVIA, Materials Studio, San Diego: Dassault Systémes, 2017.

[S15] M. D. Foster, A. Simperler, R. G. Bell, O. D. Friedrichs. F. A. A. Paz, J. Klinowski, *Nat. Mater.* **2004**, *3*, 234-238.

[S16] K.-P. Schröder, J. Sauer, M. Leslie, C. R. A. Catlow, J. M. Thomas, *Chem. Phys. Lett.* **1992**, *188*, 320-325.

[S17] J. D. Gale, A. L. Rohl, *Mol. Simul.* **2003**, *29*, 291-341.

[S18] W. Wan, CrystDiff, https://www.mmk.su.se/zou/electron-crystallography-software/crystdiff.

[S19] S. L. Mayo, B. D. Olafson, W. A. Goddard III, *J. Phys. Chem.* **1990**, *94*, 8897-8909.